Probabilistic seismic assessment of non-ductile RC buildings retrofitted using pre-tensioned aramid fiber reinforced polymer belts

Article *in* Composite Structures · October 2018

DOI: 10.1016/j.compstruct.2018.10.048

CITATIONS
4

READS
282

3 authors:

Saeid Tarfan
Amirkabir University of Technology
3 PUBLICATIONS **7** CITATIONS
SEE PROFILE

Mehdi Banazadeh
Amirkabir University of Technology
46 PUBLICATIONS **233** CITATIONS
SEE PROFILE

Mohsen Zaker Esteghamati
Virginia Polytechnic Institute and State University
9 PUBLICATIONS **13** CITATIONS
SEE PROFILE

•

How to cite this paper: Tarfan, S., Banazadeh, M., Zaker Esteghamati, M., Probabilistic seismic assessment of non-ductile RC buildings retrofitted using pre-tensioned aramid fiber reinforced polymer belts. *Composite structures***, 2018,** DOI: 10.1016/j.compstruct.2018.10.048

Probabilistic seismic assessment of non-ductile RC buildings retrofitted using pre-tensioned aramid fiber reinforced polymer belts

Saeid Tarfan[1]; Mehdi Banazadeh[2]; Mohsen Zaker Esteghamati[3]

[1]*M.Sc. Alumnus, Amirkabir University of Technology, Iran*

[2]*Associate Professor, Civil and environmental engineering department, Amirkabir University, Tehran, Iran*

[3]*Graduate Assistant, Department of Civil Engineering, University of Akron, Akron, Ohio, USA*

Abstract:

The current manuscript presents a probabilistic seismic assessment of non-ductile RC structures retrofitted by pre-tensioned aramid fiber reinforced polymers (AFRP). Three RC buildings with different heights (4-, 6- and 8-stories) are designed according to older construction practice and the poorly detailed columns of each model are then retrofitted using pre-tensioned AFRP belts. The numerical finite element models are developed in OpenSees using concentrated plastic hinge models that can capture shear weakness of original columns and deterioration of beams' stiffness and strength. Incremental dynamic and nonlinear static analyses are performed to quantify structures' performance in terms of both global- and component-level metrics. The structures' global response is evaluated using fragility curves, mean annual frequency of collapse, and collapse margin ratios. Furthermore, statistical analyses are performed to obtain median inter-story drift distribution along the height of the structure, structural members' ductility and dissipated energy under three different seismic hazard levels. The results indicate that retrofitting by pre-tensioned AFRP improves the structure's global-level ductility and reduces the collapse probability significantly. Moreover, it can prevent weak story formation by engaging a larger number of stories in collapse mechanism. From a component-level perspective, pre-tensioned AFRP increases columns' ductility and dissipated energy and enhances their performance, particularly at near-collapse-limit states.

Keywords: Shear Failure, Seismic Retrofitting, Pre-tensioned AFRP, Fragility Curves, Incremental Dynamic Analysis, Performance-based Earthquake Engineering

1. Introduction

During recent earthquakes, such as L'Aquila in 2009 and Christchurch in 2011, reinforced concrete (RC) buildings were severely damaged due to shear-, plastic hinge-, splice- and anchorage-failure of their columns [1,2]. Among these mechanisms, shear failure is particularly common in older RC buildings, since their columns are either inadequately detailed with widely spaced hoops or only designed for gravity loads. Shear failure reduces columns' ductility and axial load-bearing capacity, and hence imposes additional gravity loads to adjacent structural members, which can lead to partial or entire structural collapse. As previously shown by Liel et al., a non-ductile RC frame structure at a high-seismic site in California is 40 times more likely to collapse than a code-complying ductile one [3]. Such a high probability of collapse and its socioeconomic impacts on the large stock of non-ductile buildings around the world urges the need for simple, low-cost and efficient retrofitting techniques.

In the last two decades, fiber reinforced polymers (FRPs) have become increasingly popular in the retrofitting of concrete and masonry buildings because of their low weight-to-strength ratio, corrosion resistance, high tensile strength and easy handling [4,5]. In addition, FRPs can be pre-tensioned, which increases the yield load of the transverse reinforcement and improves the load-bearing capacity of the retrofitted RC member. Also, pre-tensioned FRPs increase concrete initial stiffness, delay concrete core expansion, control crack width, and reduce the strain level of longitudinal reinforcement, which consequently improves FRP efficiency [6,7]. The effect of FRP on the behavior of concrete columns has been widely studied [8–10] and Table.1 summarizes several of these studies. As shown in Table 1, these studies suggest that FRP increases the lateral load and drift capacity of RC columns that are not seismically designed [11].

A major shortcoming of the current literature is that limited studies addressed the global response of FRP-retrofitted structures, instead of focusing on a single column or beam. Given the importance of this issue, Di Ludovico et al. [12] evaluated an under-designed RC structure retrofitted with FRP. They showed that retrofitted frame could sustain a higher value of peak ground acceleration than the under-designed frame. Eslami and Ronagh [13] investigated the effect of FRP wraps on seismic performance of two 8-story RC frames with different column stirrup details. They showed that FRP wraps increased the ductility and seismic resistance of the poorly confined frame. Cao and Ronagh [14] performed damage analyses on an 8-story RC frame retrofitted by FRP subjected to different seismic excitations. They observed that the damage index of the poorly confined frame was reduced significantly under all different seismic intensities. In addition, they reported that retrofitted models had lower damage indices than the code-compliant intermediate frames. Niroomandi et al. [15] compared performance level of ordinary RC frames with FRP-retrofitted joints. They concluded that FRP-retrofitted joints increased lateral load resistance of an ordinary frame to the extent of an intermediate frame.

Despite the significance of the aforementioned studies, these studies' scope is limited to only few global response metrics, e.g., ductility reduction factor, which are not incorporated into the current state-of-the-art framework of performance-based earthquake engineering (PBEE). PBEE is a conditional probabilistic framework to assess performance using quantitative metrics. In PBEE, numerical models of structures are typically subjected to a suite of ground motion records to perform nonlinear response history analysis, and the model response is then recorded. Next, the probability distribution of exceeding a specific response level, conditioned on the seismic

excitation intensity, is determined. This conditional probability, denoted as seismic fragility, can be used to compare structural performance or is integrated over the ground motion intensity distribution of the site to represent annualized seismic risk of the model [16,17]. The incorporation of PBEE-compatible approaches for assessment of FRP retrofitting is a critical step for future resilience-based risk mitigation of vulnerable communities [18]. In addition, unlike other common FRPs, the application of pre-tensioned aramid FRPs (AFRPs) for seismic retrofitting of RC frames has not been explored to date. As will be discussed in section 2, pre-tensioned AFRPs provide practical and structural advantages, and further research is needed to better understand their effects on the seismic response of older RC frames.

The current manuscript presents a comprehensive seismic assessment of RC structures retrofitted with pre-tensioned AFRPs from both global- and component-level perspectives. The experimental results of AFRP-strengthened columns, carried out by the second author [19], is implemented into the PBEE framework to investigate the response of non-ductile RC buildings from elastic state to collapse. In this study, three 4-, 6- and 8-story buildings are designed according to old construction practices, and the critical regions of columns are assumed to be retrofitted, following a technique described in Section 2. Nonlinear numerical models are developed in OpenSees, and incremental dynamic and nonlinear static analyses are performed. The results are used to derive fragility curves, mean annual frequency of collapse, and collapse margin ratio (CMR). Finally, the inter-story ratio (IDR) distribution along the height of buildings, and median ductility and dissipated energy values of columns and beams are calculated under design basis earthquake (DBE), maximum considered earthquake (MCE), and collapse hazard levels, and compared between the original and retrofitted buildings. The result of this study can provide a better understanding of the pre-tensioned AFRP application to retrofit older RC structures under a wide range of seismic hazard intensities. In addition, it bridges the current literature's gap between the local effects of FRP material and the structure's overall seismic risk. Lastly, the numerical models are consistent with PBEE framework and can be readily implemented in resilience-based evaluation of communities consisting of non-ductile building portfolio.

2. Retrofitting method

Since the first use of FRPs to retrofit RC bridges in 1987 [4], different externally bonded FRP materials have been used to upgrade RC structures' flexural and shear performance. Three common FRP materials in civil engineering practice are carbon (CFRP), glass (GFRP) and aramid (AFRP) FRPs. CFRPs show the best mechanical properties such as the highest tensile strength and modulus of elasticity [20]. Previous studies have shown that CFRPs can reduce collapse potential of non-seismically designed RC bridge piers [21], improve the strength and energy dissipation of beam-column subassemblages [22], and reduce the seismic demand of frames with retrofitted infill walls [23]. On the other hand, while GFRPs have the lowest stiffness and tensile strength, they are the least expensive. GFRPs have been used to repair and strengthen RC beams [24], increase strength and deformation of masonry houses [25], and serve as a reinforcement cage in precast concrete tunnel segmental lining [26] . While AFRPs are less explored than the two other FRPs, nevertheless they exhibit favorable features such as excellent dielectric, flame resistance, and fast curing time [27]. The tensile strength and stiffness of AFRPs are higher than GFRPs. In addition, comparing to CFRPs, AFRPs provide several practical advantages such as easier handling and installment, higher work speed, and better rounding of corner angles when applied to beams and columns [28]. Besides their difference in terms of mechanical properties and application, these

FRP materials have different long-term performance and durability under environmental effects. For example, while CFRP is not affected by moisture, GFRPs and AFRPs are susceptible to mechanical degradation due to moisture ingress [29]. Although CFRP generally shows the best durability characteristics, AFRP significantly outperforms GFRPs in regard to Alkali resistance and fatigue [30]. To conclude, although each FRP material provides a distinctive advantage for a particular retrofitting application, AFRPs provide high workability and favorable mechanical and durability characteristics.

In this study, it is assumed that the emergency retrofit method proposed by Yamakawa and Banazadeh [19] is used to strengthen non-ductile columns of the under-designed buildings. This technique uses AFRP belts. Figure 1 shows the schematic detail of this retrofitting method. As shown in Figure 1, two-ply aramid belts are twisted around the non-ductile columns. The ends of each ply form a hook, which is later secured using crossbar and bolts. The pre-tensioned force is applied manually by fastening the belts. The width and thickness of aramid plies are 17 *mm* and 0.61 *mm*, respectively, and the spacing between each belt is taken as 100 mm. A pre-tensioning force of 688 MPa is applied to bolts. Two major advantages of this technique are easy installation and the ability to readily apply or adjust pre-tensioning stress to a specific pre-tensioning stress level, which increases the potential of this technique for rapid structural rehabilitation before or after an earthquake scenario. The second author had completed a series of cyclic tests on shear-critical columns and showed that the proposed technique effectively restores seismic performance of damaged columns. The retrofitted columns sustained larger axial force and recovered from 60% up to 100% of concrete cylinder strength. Also, the active confinement of pre-tensioned AFRPs shifted the shear failure mode to a flexural failure mode [19]. `

3. Numerical Modeling

3.1. Seismic design of prototype buildings

Three 4-, 6- and 8-story RC buildings are designed according to ASCE 7-10 [31] and ACI 318-08 [32] minimum requirements. The designed prototype buildings present the expected design variation of short- and medium-rise buildings in California's construction practice prior to 1970 [3]. Figure 2 shows the typical layout plan and elevation of the buildings. Each building consists of perimeter moment-resisting frames (MRFs) in both directions. Floor slabs are modeled using membrane elements that provide a load transfer path and constrain the interior gravity frames and the perimeter MRFs. The columns are assumed to be fixed at the base. The prototype plans consist of three and four bays in each direction. The typical story height and bay width are 3.2 m and 4.5 m, respectively. Dead and live load values of 5.89 kN/m^2 and 1.96 kN/m^2 are assigned to all buildings floors, respectively. Concrete compressive strength is assumed as 25 MPa and longitudinal and transverse reinforcement with yield strength values of 400 MPa and 300 MPa are used, respectively.

The buildings are assumed to be located in Los Angeles, California with latitude and longitude of 34.05°N and 118.24°W, respectively. Based on the site hazard map, prototype buildings should meet the seismic design category D requirement (the highest seismic vulnerability) with a risk category of II (for common residential units) and stiff soil site class D, which corresponds to the maximum considered earthquake (MCE) spectral acceleration at short periods (S_s) and 1s period (S_1) of 2.43g and 0.85g, respectively. In order to imitate older RC structures construction and achieve non-ductile columns, the MRFs are designed without

considering two requirements of seismic design category D. First, instead of using special MRFs that are required for this design category, intermediate MRFs are selected. Intermediate MRFs have less stringent detailing requirements than special MRFS and they exhibit moderate ductility. Second, section 21-3 of ACI 318-08 requirements for columns are deliberately discarded. Ignoring this requirement resulted in widely spaced hoops in columns. Therefore, the designed buildings represent "inadequately detailed" RC buildings in the real world. Other requirements of ASCE 7 for ordinary MRFs are met, namely, minimum and maximum longitudinal reinforcement ratio and spacing, required flexural strength of frame sections, and maximum inter-story drift ratios. Since all the prototype structures are short-period (less than 3.5 s) and have no horizontal and vertical irregularity, equivalent lateral force (ELF) analysis is performed. Based on ASCE 7, the response modification coefficient (R), and deflection amplification factor (C_d) of intermediate MRFs are taken as 5 and 4.5 in ELF analysis, respectively. ELF analysis treats structure as a single-degree-of-freedom system with a period corresponding to the first mode of the structure and obtains the corresponding spectral acceleration from an elastic design spectrum. The resultant elastic seismic response is then reduced using R to account for the nonlinear behavior of the structure. Furthermore, the displacement values (in terms of maximum inter-story drift) are amplified using Cd to ensure that the design accounts for large nonlinear displacements of the structure. The seismic design results of the buildings are shown in Table 2. As shown in Table 2, buildings are designed for the seismic coefficient (C_s) values from 0.09 to 0.18 and their fundamental periods (T_1) range from 0.65 s to 1.2 s. Table 3 summarizes the designed sections of beams and columns for the prototype buildings.

3.2. Nonlinear finite element modeling

Two-dimensional finite element models of RC moment-resisting frames are developed in OpenSees simulation platform [33]. Figure 3 shows the configuration of nonlinear models. The P-Δ effect of gravity frames is considered through a leaning column, where the seismic weight of interior frames is assigned to a pinned column. The leaning column is connected to the moment-resisting frame using rigid truss elements. In order to quantify the effect of pre-tensioned AFRP retrofitting technique, two different nonlinear models are prepared for each building. The numerical model consisting of non-ductile columns is denoted herein as "original" building, whereas the same building when strengthened with pre-tensioned AFRP belts is referred as "retrofitted" structure.

In the original buildings, non-ductile columns are modeled using an elastic element with plastic hinges at both ends. The plastic hinge is comprised of two shear and flexural subelements, following the numerical procedure by Yamakawa and Banazadeh [34] (Figure 3). The flexural subelement is defined by fiber sections, where column cross-section is discretized to uniaxial concrete and longitudinal reinforcement fibers. *Concrete01* material is used for cover and core concrete in OpenSees which accounts for degrading of concrete stiffness and ignores its tensile strength [33]. The shear subelement behavior is defined based on a modified shear-distortion relation using the *hysteretic* material in OpenSees. As shown in Figure 4, the monotonic shear-distortion behavior is initially defined according to the MCFT and adjusted based on a procedure described in [19]. Then, the point corresponding to half of the shear strength from MCFT model at 0.4% shear distortion is connected to shear strength value of the Pan and Li equation, as follows [35]:

$$V_n = k_\mu (1 + \frac{K_a}{K_t}) V_{ct} + (1 + \frac{k_\mu K_a}{K_t}) V_s \quad (1)$$

Where V_n, V_s, and V_{ct} show the shear strength of column, transverse reinforcement, and concrete, respectively, μ_k, K_a, and K_t represent the ductility effect coefficient, stiffness of truss, and stiffness of arch components defined in [35].

In the "retrofitted" buildings, shear subelements of columns are discarded and the pre-tensioned AFRP effect is considered as active and passive confinement in flexural subelement using Mander's confinement model [36], following [19] suggestion. The active confinement is due to the pre-tensioning stress of AFRP belts as follows:

$$\sigma_r = \frac{n a_a}{s_a b} \sigma_p \quad (2)$$

where σ_r and σ_p show active confinement and pre-tensioning stresses respectively. a_a, s_a, n and b show the area of a single AFRP ply cross-section, AFRP belts spacing, number of AFRP plies and column width, respectively. The active confinement stress is then used to adjust the concrete compressive stress in the Mander's equations based on [37]. AFRP passive confinement is determined as the working stress corresponding to strain value of 0.7% [34]. Therefore, retrofitted columns are confined by three different sources: active confinement of AFRP belts due to pre-tensioning, passive confinement of widely spaced hoops, and passive confinement of AFRP belts. Figure 5 compares the effect of different confinement sources on the stress-strain curve of a 50 cm x 50 cm concrete section. The unconfined concrete, such as cover concrete, shows a baseline to compare other confining methods. The "poorly confined" line (denoted with a dotted line) shows the effect of insufficient transverse reinforcement of original model on the behavior of concrete. On the other hand, the "retrofitted concrete" line (denoted with a dashed line) shows that the combination of all three sources in the retrofitted buildings. As Figure 5 shows, while the poorly confined provides a minimum level of ductility, the confinement due to AFRP retrofitting increases both strength and ductility of the concrete, and such effect is significantly larger for the ductility.

In both retrofitted and original buildings, beams are modeled using elastic elements with two flexural inelastic springs at their ends. The elastic part and springs are modeled by *elasticBeamColumn* and *zeroLength* elements in OpenSees, respectively. The inelastic spring behavior is defined using Ibarra-Medina-Krawinkler (IMK) model. This model is able to account for both monotonic and cyclic deterioration of structural members when they are damaged. Five parameters are needed to construct the trilinear backbone curve of IMK model: yield moment (M_y), capping strength (M_c), yield stiffness (k_y), pre-capping plastic rotation (θ_p), and post-capping plastic rotation (θ_{pc}). An additional parameter, deterioration parameter (λ), is then used to capture the cyclic degradation of beam's stiffness and strength during an earthquake simulation. The aforementioned parameters are derived based on the regression equations developed by Haselton et al [38].

In both retrofitted and original buildings, the beam-column connections are modeled using the *Joint2D* element in OpenSees. This element creates four constrained external nodes to connect the adjacent frame member to the panel zone, while a central *zerolength* element defines the panel zone shear behavior [39]. The damping is defined using the Rayleigh model by assigning 5% of critical damping ratios to the first and second vibration modes of buildings computed from the eigen analysis. In order to resolve convergence and damping issues of plastic hinge models, the stiffness of plastic hinges, and elastic part are modified, based on Zareian and Medina's recommendations [40].

3.3. Verification of the numerical model

In order to verify the accuracy of the proposed procedure, the finite element model is compared to the experimental study of retrofitted columns by the Yamakawa and Banazadeh [34]. In this experiment, a 250 *mm* x 250 *mm* x 750 *mm* rectangular column (A0 specimen) with shear span to depth ratio of 1.5 and transverse reinforcement of 0.08% was subjected to a cyclic test with three cycles at drift angle ratios of 0.5%, 1%, 1.5%, 2%, 2.5%, and 3% followed by a single cycle at 4% and 5% drift angle ratios under constant axial force ratio of 0.2. In addition, three other specimens with the same dimensions were tested, where the axial load was kept at a constant level and the damaged column was then retrofitted with 2-ply AFRP belts with 200 *mm* spacing (A200/3 specimen), 2-ply AFRP belts with 65 mm spacing (A65/2 specimen) and 2-ply AFRP belts with 65 mm spacing (A65/3 specimen), respectively. The axial force ratio was kept at 0.2, 0.2, and 0.4 for the A200/3, A65/2 and A65/3 specimens, respectively. The yield strength and elastic modulus of aramid fiber belts were 2065 *MPa* and 118 *GPa*, respectively, and they were wound in 17 mm width parallel belts. The ends of the plies were then secured using a crossbar, and 688 *MPa*, 1032 *MPa* and 688 *MPa* of pre-tensioning force was applied to the A200/3, A65/2 and A65/3 specimens, respectively. In OpenSees, the specimen column was modeled based on the procedure described earlier and a displacement-control analysis with modified Newton algorithm was employed, following the experiment cyclic load pattern. Figure 6 shows the comparison between numerical and experimental results.

In order to quantify the difference between the finite element models and test results, the average of maximum strength and drift of each cycle are compared. Overall, for shear-critical columns, the difference between the displacement of finite element model and test are lower than same values for strength. For the A0 specimen, the differences between OpenSees's average strength and the test's average strength are 12% and 15% at positive and negative branches of hysteresis, respectively, whereas the differences between drifts of OpenSees and test results are 3% and 1.5% at the positive and negative branches, respectively. The larger difference in strength is due to shear failure mode, which renders fiber finite element model ineffective to account for bond slip and rebar pullout, thus reducing its accuracy. For A200/3 specimen OpenSees predicts average strength 15% and 18% higher than the test's average strength at positive and negative branches of hysteresis, respectively, whereas for the drift, OpenSees's estimation is 6% and 7% lower than the test results at the positive and negative branches, respectively. It should be noted that the large spacing of this specimen results in a mixed shear/flexural failure mode and as a result, the difference in finite element model and test results is similar to the unreinforced specimen. On the other hand, when members experience a flexural mechanism, the agreement between finite element model and test results increases, particularly for strength. For A65/2 specimen, the differences between OpenSees's average strength and the test's average strength are 7% and 8%

at positive and negative branches of hysteresis, respectively, whereas the difference between drifts of OpenSees and test results are 8% for both positive and negative branches. For A65/3 specimen OpenSees's estimates the average strength 11% and 8% lower than the test's average at positive and negative branches of hysteresis, respectively, whereas the difference between drifts of OpenSees and test results are 11% and 12% at the positive and negative branches, respectively.

As shown in Figure 6, the numerical model has a satisfactory accuracy to predict the behavior of original shear-critical column before and after retrofitting. Although there are some small discrepancies at higher displacement, it is well-known that finite element models are usually stiffer than the actual specimen [15]. Therefore, numerical results are in good agreement with experimental results as they trace maximum load resistance and the general trend of the experimental observation.

4. Nonlinear Analysis

4.1 Pushover analysis

Pushover analysis is performed using the inverse triangular load pattern described in ASCE 7-10 [31]. In this method, the displacement of a roof node is monotonically increased, and the base shear change is recorded. Figure 7 compares the pushover curves of original and retrofitted buildings. As shown in Figure 7, for all different building heights, the original model shows a brittle shear failure mechanism, whereas the retrofitted model exhibits a ductile response. Furthermore, the retrofitted buildings have significantly larger ductility and strength compared to original ones.

To quantify the difference between models' strength and ductility, static overstrength (Ω), and period-based ductility (μ_T) values are determined from pushover analysis and are reported in Table 4, respectively. The static overstrength factor is the ratio of maximum base shear from pushover analysis to the design base shear. As shown in Table 4, static overstrength values of all the retrofitted models are larger than the original models. The static overstrength value of the retrofitted model is 29.5%, 60.5%, and 44.9% larger than the original model for 4-, 6- and 8-story buildings, respectively. Period-based ductility is defined as the ratio of the global ultimate displacement corresponding to the point of 20% strength loss to global yield displacement. In all different building heights, the retrofitted model has a significantly larger ductility compared to the original model. The μ_T of retrofitted 4-, 6- and 8-story buildings are 137.2%, 71.1% and 194.8% larger than the original models with the same height. Overall, retrofitting with pre-tensioned AFRP belts increases both ductility and overstrength but its impact on the ductility is more substantial.

4.2. Incremental dynamic analysis

Incremental dynamic analysis (IDA) is a numerical simulation technique which captures the structure's seismic response from elastic state to collapse. In this method, a suite of ground motion records is selected and time history analysis is performed by repeatedly scaling each record's intensity measure until the structure's failure [41]. An IDA plot is then plotted by recording an engineering demand parameter of interest versus the ground motion intensity measure. In this study, 44 far-field ground motion records of FEMA P695 are used [42]. This ground motion suite consists of strong ground motion records from earthquakes with magnitude and distance larger than 6.5 and 10 Km, respectively. Maximum inter-story drift ratio ($IDR_{\max}$) and spectral acceleration at structure fundamental period (S_a) are recorded as structure demand

parameter and ground motion intensity measure, respectively. Collapse point is identified either as numerical instability where a trivial increase in ground motion intensity measure will cause a large increase in the response, reaching a pre-defined upper bound of the response (here taken as inter-story drift ratio that exceeds 10%) or when the tangent slope of IDA curve is 20% of the elastic slope. “Hunt and Fill” algorithm is employed to reduce computational demand of the analysis while maintaining its accuracy [43].

Figure 8 compares the median IDA curves of the buildings. As shown in Figure 8, at lower ground motion intensities, e.g. S_a value less than 0.2 g, both original and retrofitted models have similar behavior since AFRP belts are possibly not engaged yet. However, as the shaking intensity level increases, the original building reaches to its collapse capacity rapidly, whereas the retrofitted building resists a significantly larger seismic demand. In order to quantify their difference, the spectral acceleration values of median IDA curves are compared at different limit states in Table 5. Based on FEMA 356 guideline [44], immediate occupancy (IO), life safety (LS), and collapse prevention (CP) limit states of concrete frames are defined when the maximum inter-story drift value exceeds 1%, 2%, and 4%, respectively. A “collapse" limit state, which refers to the $IDR_{\max}$ value, corresponding to collapse point in IDA analysis, is also included. In this regard, CP limit state represents severe damages and onset of collapse, whereas “collapse” limit state shows the expected actual collapse due to dynamic instability. Table 5 presents the median values of S_a at IO, LS, CP and collapse for the original and retrofitted models. As shown in Table 5, the AFRP retrofitting does not influence IO and LS limit states significantly, whereas CP and collapse limit states are affected notably. For example, the 6-story retrofitted model exceeds CP and collapse limit states at S_a values that are 22.6% and 48.0% larger than the original model, whereas both models exceed the IO limit state at the same Sa value. The same trend can be observed in other buildings. This interesting observation will be further discussed in the next section.

5. Seismic Performance Assessment

5.1. Fragility evaluation

Seismic fragility is the probability of a building’s response exceeding a particular limit state, conditioned on the ground motion intensity measure [45]. Here, the fragility function is defined as follows:

$$P(IDR_{\max} > IDR_{\max}^{k} \mid S_a = S_{ai}) = \Phi\left(\frac{\ln(\frac{S_{ai}}{\mu})}{\sigma}\right) \quad (3)$$

where S_{ai} and $IDR_{\max}$ are the S_a value of i^{th} ground motion spectral acceleration and structure’s maximum inter-story drift values, respectively. $IDR_{\max}{}^{k}$ shows the maximum inter-story drift associated with the k^{th} limit state. Φ, μ, and σ are a standard normal cumulative distribution and its mean and standard deviation, determined from IDA results.

When the same suite of ground motion is used to evaluate a number of numerical models, the fragility results, especially for higher hazard levels such as collapse, should be adjusted to

account for the difference between the spectral shape of the applied ground motion suite and the site-specific spectral shape [46,47]. The second method described in [47] is used to adjust the median and standard deviation of fragility curves based on the hazard deaggregation results of Los Angeles, following a set of empirical equations for FEMA far-field suite. Figure 9 compares the adjusted collapse fragility curves of the retrofitted and original buildings. In all buildings, for a given S_a value, the retrofitted model has a lower probability of collapse, compared to the original model. The median values of collapse fragility curves, denoted as S_{aCol} in Table 4, show the S_a values where half of the selected ground motion records will cause the building to collapse. As Table 4 shows, retrofitting with pre-tensioned AFRP increases the $S_{a\mathrm{Col}}$ value, i.e. the median collapse capacity, significantly in all different building heights. For example, the median collapse capacity of the retrofitted 4-story building has an increase of 119.0% compared to the original building. This is consistent for 6- and 8-story buildings where the retrofitted structures have median collapse capacities that are 66.7% and 83.6% larger than the original buildings, respectively.

In order to elaborate the effect of retrofitting with pre-tensioned AFRP at different damage states, IO and LS fragility curves are derived following the same formulation described in Equation 3. Figures 10.a to 10.c compare the IO and LS fragility curves of the 4-, 6- and 8-story models, respectively. As shown in Figure 10, despite the significant effect of pre-tensioned AFRP on collapse capacity of the studied buildings, its effect on limit states corresponding to slight to moderate damage states is negligible. For example, the difference between fragility curves of the 6-story original and retrofitted models are less than 5% for both IO and LS limit states. It can be concluded that retrofitting using pre-tensioned AFRP affects structure global seismic response, but its impact depends on the considered limit state; when a structure experiences near collapse limit state, the AFRP retrofitting is more effective.

5.2. Collapse assessment

As mentioned in section 3.2 and 4.1, the effect of AFRP retrofitting is more substantial at collapse limit state. Therefore, this section addresses collapse limit states of retrofitted and original models using quantifiable metrics. Table 4 reports four collapse metrics: the median value of maximum inter-story drift ratio at collapse (IDR_{col}), the probability of collapse at maximum considered earthquake level ($P[C|S_{\mathrm{aMCE}}]$), mean annual frequency of collapse (λ_{col}) and the probability of collapse in 50 years ($P_{C/50}$). As shown in Table 4, the retrofitted model has larger IDR at collapse comparing to the original model, which indicates that the retrofitted model has higher global-level ductility. This is consistent with the period-based ductility results discussed in Section 3.1. For example, the original 4-story model reaches collapse at median IDR value of 5% while the retrofitted model reaches the predefined upper bond of 10%, showing a significantly large deformation at collapse. The probability of collapse conditioned on the occurrence of MCE is drastically reduced for all the retrofitted models and even reaches the acceptable 10% threshold of ASCE 7-10 in most cases. For example, AFRP retrofitting reduced collapse probability at MCE of the 4-story building from 70% to 6%. The same observation can be made for other structures. Although the retrofitted 6-story model has a $P[C|S_{\mathrm{aMCE}}]$ value larger than 10%, its initial collapse probability is reduced by 215.8%.

Mean annual frequency (MAF) of collapse is obtained by multiplying the intensity measure hazard curve with the conditional probability of collapse (i.e. Collapse fragility curve) and

integrating over the whole range of the intensity measure. Therefore, this metric covers the structure's performance in a larger range comparing to $P[C|S_{aMCE}]$ which only considers MCE. In this study, discrete 5% damped S_a hazard values are obtained from USGS unified hazard tool for the site of interest, and a polynomial is fitted for each building. Figure 11 shows the interpolated S_a hazard curve of the buildings, which represents the mean annual frequency that the site's S_a exceeds a given value. As shown in Figure 11, MAF of exceeding S_a is a function of first mode period and is smaller for the building with a longer fundamental period. Subsequently, the MAF of collapse is obtained as follows:

$$\lambda_c = \int_{S_a=S_a^1}^{S_a=S_a^2} P(C \mid S_a) \left| \frac{d\lambda_{S_a}}{dS_a} \right| dS_a \tag{4}$$

where λ_{Sa} refers to the MAF of S_a exceedance, and $P(C| S_a)$ shows the probability of collapse for a given S_a As shown in Table 4, MAF of the collapse of original models ranges from 9.04 $x10^{-4}$ to 14.98$x10^{-4}$, whereas the collapse MAF values of the retrofitted models are reduced to roughly one-third of the original models, ranging from 2.83 $x10^{-4}$ to 4.82$x10^{-4}$. Finally, the collapse probability in 50 years is calculated based on MAF of collapse results. ASCE 7-10 requires collapse probability in 50 years to be lower than 2%. As shown in Table 4, all the original models have significantly higher collapse probability in 50 years than the acceptable threshold; however, the retrofitted 4- and 8-story models collapse probability in 50 years are below 2%. Similar to other metrics, the 6-story retrofitted model has a collapse probability in 50 years of 2.4%, which is slightly over the acceptable threshold. Further discussion on the 6-story retrofitted model will be presented in the next section. To conclude, all the metrics suggest that retrofitting with pre-tensioned AFRP is an effective technique to reduce collapse probability of non-ductile RC structures, though there is no guarantee that the improved collapse behavior of the retrofitted buildings will be within the acceptable range of modern seismic codes.

5.2.1 FEMA P695 assessment

The procedure of Federal Emergency Management Agency (FEMA P695) [42] is also used to compare buildings' collapse performance to an allowable threshold. This procedure assesses whether a structure has an adequate safety margin against collapse under the MCE, defined as collapse margin ratio (*CMR*). CMR is the ratio of median collapse capacity, $S_{a,col}$, to the spectral acceleration at the MCE level, S_{aMCE}. Since the spectral shapes of the FEMA P695 records do not match the site of buildings and their period, the CMR values are adjusted using spectral shape factor (*SSF*). SSF values are determined based on structures' period-based ductility and fundamental period of structures and are multiplied by CMRs to obtain the adjusted CMRs (ACMRs). Lastly, the computed ACMRs are compared to the allowable ACMR, which is determined based on an acceptable collapse probability of 10% and the total collapse uncertainties associated with the nonlinear finite element models, structure design requirements and materials, and record-to-record uncertainty.

Table 6 presents the results of FEMA P695 assessment. It is important to mention that the CMR values represented in Table 6 are obtained from unmodified collapse fragility curves, since they are later adjusted based on SSF values in a similar manner to the second method described by Haselton et al. in [47]. The original models fail to provide an adequate safety margin against collapse (CMR≤1) due to the fact that their collapse capacity is actually smaller than the MCE

demand, which subsequently reflects in their unacceptable ACMRs. On the other hand, the AFRP retrofitting increases the numerator of CMR ratio, providing the acceptable safety margin in most cases. This is not surprising because both ductility (which is reflected in higher SSF) and CMR values of the retrofitted models are significantly larger than the original models. Consistent with the previous collapse metrics, although the ACMR of the retrofitted 6-story model is increased by 65.82%, this building fails to provide the acceptable safety margin, mainly because of its lower increase in ductility compared to other buildings. In order to elaborate on this observation, it should be noted that pre-tensioned AFRP improves non-ductile RC frames behavior by mostly increasing their ductility. Therefore, the effectiveness of the retrofitting technique lies in the extent of the additional ductility that it provides. As mentioned in section 4.1, the 6-story has the lowest increase in ductility in comparison to the other two buildings (71% versus 137.2% and 194.8%, respectively). This lower improvement is reflected in SSF coefficients (1.06 comparing to 1.19 and 1.26 for 4- and 8-story models, respectively) which is later multiplied by the CMR. Therefore, while the CMR of the 6-story is improved (from being less than one to being more than one), the retrofitted model does not provide a similar ductility as expected for a modern 6-story building in this seismic zone. The difference in the increased ductility could be due to the design variation of the studied models. In other words, pre-tensioned AFRPs increased the stiffness of non-ductile columns of the 6-story frame to an extent that it actually reduced the ductility of columns at collapse. In addition, the transverse ties of the 6-story model's columns are smaller than the two other models, which lead to smaller post-capping rotation capacity and subsequently smaller initial ductility of columns. Since the initial ductility is lower, the final improved ductility could not reach a satisfactory level. This indicates that the effect of AFRP retrofitting is sensitive to the seismic detailing and could be more substantial for a particular design. The variation in building design and geometry leads to different collapse mechanism and if other structural members play a significant role in the collapse as well, then the sole seismic upgrade of columns' ductility plays a smaller role in the overall collapse response of the structure.

5.3. Comparison of structural performance at different hazard levels

In this section, the results of IDA are used to derive the median inter-story drift distribution, structural members' ductility, and dissipated energy at three different hazard levels—DBE, MCE and collapse levels. DBE and MCE earthquakes are defined as S_a values with 10% and 2% exceedance probability in 50 years at the site of interest based on the Los Angeles response spectrum, respectively. Since the period of original and retrofitted models are equal, they undergo the same S_a demands under DBE and MCE, providing a comparable basis to assess pre-tensioned AFRP effect under low and high seismic intensities. Additionally, collapse S_a value corresponds to median collapse capacity; which is different for the original and retrofitted models and represents how each model responds at near collapse limit state.

5.3.1. Story drift distribution

Figure 12 compares the distribution of median IDR along the height of 4-, 6- and 8-story buildings, respectively. As shown in Figure 12.a and 12.b, IDR of the original 4-story model at lower stories is higher than the retrofitted building under both DBE and MCE, indicating lower stiffness of the original model. Also at MCE level, a weak story is formed at the second floor of

the original model (Figure 12.b), whereas the retrofitted model reduces IDR of the second floor to half of the original one.

Figures 12.d and 12.e show that the excessive drift is accumulated on the second floor of the original 6-story model, whereas both first and second floors are engaged in the collapse mechanism of the retrofitted model. The higher number of engaging stories indicates better performance of columns to redistribute forces in the retrofitted building. This issue is better shown in Figure 12.f, where all the top four stories of the original 6-story building have nearly the same low IDR at collapse whereas the second floor shows a significantly larger drift, indicating a possible weak story formation. On the other hand, the 6-story retrofitted model exhibits large drift at lower two stories, showing a more ductile response.

Figure 12.g shows that at DBE level, both original and retrofitted 8-story models have the same IDR at lower stories. However, the original model has a larger IDR at the sixth story compared to the retrofitted one. As shown in Figure 12.h, a weak story is formed at the sixth story of the original model under MCE, whereas the retrofitted 8-story building has nearly the same IDR at the top four floors. Lastly, Figure 12.i shows that retrofitting with pre-tensioned AFRP has changed the collapse mechanism of the 8-story buildings and the first, second and third stories of the retrofitted model are engaged in the collapse mechanism, whereas only the sixth floor of the original building exhibits a significantly large IDR.

Overall, at collapse level, retrofitting with pre-tensioned AFRPs increases the IDR compared to the original, which indicates that the retrofitted models have higher ductility. In addition, while weak stories are formed in the original buildings, retrofitted buildings show different collapse mechanisms with more stories engaged in the collapse mechanism.

5.3.2. Frame member's ductility

Table 7 presents median values of frame components' ductility. Component ductility (μ) is defined as the ratio of plastic deformation to the yield deformation of a structural member. As shown in Table 7, the 4-story retrofitted model has lower ductility at the first floor, whereas, at upper stories, its columns and beams show higher ductility in comparison to the original model at DBE level. The 4-story retrofitted model has higher ductility at all floors under MCE and, the difference is significantly larger when columns of the second floor and beams of the third floor are compared between these models. At collapse level, columns of the second floor in both models show large ductility consistent with the collapse mechanism observed in Figure 12.c. However, the retrofitted models show larger values of components' ductility at all floors. It is noteworthy that pre-tensioned AFRP resolves low ductility issues of first and third columns under MCE and collapse, though it does not affect the first floor's columns under DBE.

As shown in Table 7, retrofitting with pre-tensioned AFRP increases both columns' and beams' ductility values of the 6-story building at each story under all the considered hazard levels. The improved behavior of retrofitted models' columns leads to larger plastic deformation in beams, especially at the lower three stories. Structural components of the retrofitted 8-story model have larger ductility values at all stories, under DBE, MCE, and collapse levels. However, columns of the retrofitted model have low ductility at the first, fifth and seventh floor under DBE. Despite the fact that AFRP improved the ductility of inner columns at the fifth and seventh floors under MCE and collapse levels, the outer columns of the fifth floor still have ductility values smaller

than one. The columns of the original model lack the required ductility.Therefore, large plastic deformations are accumulated mostly at outer bays' beams. On the other hand, AFRP belts increase ductility values of columns and middle bays' beams along the height of the retrofitted model.

Collectively, retrofitting by pre-tensioned AFRP significantly increases component-level ductility in frames. However, there is no guarantee that each structural member of the retrofitted building would have an acceptable performance. For example, as shown in Table 7, the median ductility value of the retrofitted 4-story model is 23% lower than the 4-story model at the first floor under DBE. In addition, the effect of pre-tensioned AFRP is more significant at higher seismic demands. For example, at collapse level, the median ductility values of the retrofitted sixth story model are 293.8%, 131.9%, 343.3%, 82.7%, 88.2% and 152.8% larger than the original model at the first to the sixth story, respectively. Same observations can be made for the 4- and 8-story buildings at MCE and collapse hazard levels.

5.3.2. Frame members' dissipated energy

Dissipated energy is defined as the work produced by plastic deformation due to dynamic loads.The total dissipated energy of structural members' at each floor is presented in Table 8, for the studied models. As shown in Table 8, most of columns' and beams' hysteretic energy in both retrofitted and the original 4-story building is dissipated at the first and second floors, respectively, under all the considered hazard levels. However, the columns of the retrofitted model have larger dissipated energy values than the original model, whereas its beams dissipate smaller amounts of hysteretic energy.

As shown in Table 8, energy dissipation of the original 6-story model's columns is larger at the second and sixth stories under all hazard levels, whereas pre-tensioned AFRP reduces the dissipated energy of columns at the second and sixth stories and increases the dissipated energy of columns at the first story. This is consistent with the drift distribution mechanisms observed in Figure 12.f, where the original model showed an excessive drift at the second floor, while both the first and second stories of the retrofitted building were engaged in the collapse mechanism. Following the same trend, beams of the original 6-story model exhibit excessive energy dissipation at the first floor, while the retrofitted model shows higher energy dissipation at beams of the first and second floors. In addition, the dissipated energy of the retrofitted models' beams is larger at the third, fourth and fifth floors in comparison to the original model.

Table 8 shows that the dissipated energy of the original 8-story model's columns is larger at the sixth floor, while columns of the retrofitting model dissipate energy notably higher at the first and third floors under all considered hazard levels. This is similar to the pattern observed in the Figures 12.h and 12.i. In terms of beams, there is no difference in the location of maximum energy dissipation between the original and retrofitted 8-story buildings. More importantly, the same trend as the previous buildings can be noticed; pre-tensioned AFRP increases columns' total energy dissipation and reduces beams' total portion of the dissipated energy. However, this statement cannot be held true for an individual beam or column.

Overall, retrofitting by pre-tensioned AFRP increases columns' total contribution to the structure's dissipated energy and, reduces beams' energy dissipation. This indicates that columns of the retrofitted models perform better than the original models. For instance, the ratios of

column's dissipated energy to the total dissipated energy of the original 4-story are 43.5%, 45.4% and 44.3% under DBE, MCE and collapse hazard levels, respectively, whereas these ratios change to 53.3%, 61.4% and 77.0% under the same hazard levels, respectively. Furthermore, retrofitting by pre-tensioned AFRP reduces the beams' dissipated energy ratios of the original 4-story model from 56.5%, 54.6% and 55.7% to 46.7, 38.6 and 23% under DBE, MCE and collapse levels, respectively. The same observations can be made regarding the 6- and 8-story buildings.

6. Conclusion

In this study, the effect of pre-tensioned AFRPs on the global and local seismic response of three non-ductile RC buildings is investigated. The prototype buildings, ranging from 4 to 8 stories, are modeled using concentrated plastic hinge models in OpenSees. Two sets of nonlinear models are developed for the original and retrofitted cases of each prototype building, where columns behaviors are defined by a combination of adjusted MCFT shear spring with fiber flexural sub-element, and the IMK model is used to account for stiffness and strength deterioration of beams under both cyclic and monotonic loadings. The numerical models are subjected to 22 pairs of FEMA far-field ground motion records to perform IDA, and fragility curves are constructed and adjusted based on the site-specific epsilon. Different global metrics such as over-strength, MAF of collapse, and collapse probability in 50 years are obtained. Furthermore, median inter-story drift distribution at DBE, MCE and collapse hazard levels are determined and compared. Finally, from a component-level perspective, ductility and dissipated energy values of beams and columns are also calculated at the aforementioned hazard levels. The following conclusions summarize the results discussed in this study:

- Overall, pre-tensioned AFRP improves the seismic behavior of non-ductile RC buildings, and its effect depends on the considered performance level; it is shown that AFRP effect is more substantial at near-collapse-limit states.
- Based on the pushover results, pre-tensioned AFRP increases both static over-strength and period-based ductility of all the structures; however, its effect on the structure's ductility is more significant.
- The collapse fragility curves show that retrofitted models have larger median collapse capacity. However, the difference between retrofitted models and original ones are negligible at IO and LS limit states.
- Pre-tensioned AFRP significantly reduces all considered global collapse metrics (mean annual frequency of collapse, probability of collapse at MCE and collapse probability in 50 years).
- The retrofitted buildings show larger inter-story drift at collapse, indicating a ductile collapse mechanism.
- Following FEMA P695 methodology, all the original non-ductile buildings fail to meet the collapse margin ratio requirement; however, the retrofitted 4- and 8-story models provide the adequate safety margin. A similar conclusion is made when buildings are compared to ASCE 7-10 objective of 2% collapse probability in 50 years.
- The collapse findings indicated that although retrofitting with pre-tensioned AFRP improves collapse behavior of non-ductile RC structures, there is no guarantee that the retrofitted building meets modern seismic codes requirements.

- The effectiveness of the pre-tensioned AFRP retrofitting depends on the extent of increased ductility, and hence, the strength and stiffness of the frame members.
- Based on the median inter-story drift distribution, the original models show weak story formation and excessive drift accumulation at a single story, whereas retrofitting with pre-tensioned AFRP engages a larger number of stories and prevents weak story formation.
- Pre-tensioned AFRP increases both columns' and beams' ductility values, particularly at collapse level.
- In the original non-ductile buildings, more energy is dissipated at beams, whereas retrofitting with AFRP increases columns' contribution to the frame's total dissipated energy.

The results of this study support the application of pre-tensioned AFRP belts for collapse prevention of non-ductile RC frame structures at high seismic zones. While this method is inexpensive, fast, and less labor-intensive due to the high workability of AFRPs, it also reduced collapse probability of considered prototype frames by a factor of 2.5~5. Since the results obtained in this study are restricted to the particular retrofitting method and the three prototype buildings that are examined here, further research is needed to investigate the effectiveness of pre-tensioned AFRPs for other structural systems, design parameters, etc. Also, the results show that pre-tensioned AFRPs have limited effect on low damage performance levels and might not be a feasible option to upgrade structures' serviceability. In order to address lower damage levels, other retrofitting techniques can be used in combination with the proposed technique to cover a wider range of performance. Some authors[48] have shown that flexural retrofitting of beams and columns can increase the lateral strength and subsequently structural performance under low damage states. However, it should be noted that a single retrofitting scheme cannot upgrade the structure under all considered performance levels and the practicing engineer should consider the applicability of each technique for the target performance level and the underlying interactions of these techniques. Lastly, the established procedure could be easily extended to other FRPs (such as CFRP or GFRP) and structures (e.g. dual system, masonry) to evaluate the impact of different retrofitting methods and/or FRP materials on these structures. Such efforts could be substantial to better understand the challenges of structural rehabilitation from both engineering practices and natural hazard research community perspectives.

References

[1] Triantafillou T. Seismic retrofitting of structures with fibre-reinforced polymers. Prog Struct Eng Mater 2001;3:57–65. doi:10.1002/pse.61.

[2] Jeon JS, Lowes LN, DesRoches R, Brilakis I. Fragility curves for non-ductile reinforced concrete frames that exhibit different component response mechanisms. Eng Struct 2015;85:127–43. doi:10.1016/j.engstruct.2014.12.009.

[3] Liel AB, Haselton CB, Deierlein GG. Seismic Collapse Safety of Reinforced Concrete Buildings. II: Comparative Assessment of Nonductile and Ductile Moment Frames. J Struct Eng 2011;137:492–502. doi:10.1061/(ASCE)ST.1943-541X.0000275.

[4] Bakis CE, Bank LC, Brown VL, Cosenza E, Davalos JF, Lesko JJ, et al. Fiber-Reinforced Polymer Composites for Construction—State-of-the-Art Review. J Compos Constr 2002;6:73–87. doi:10.1061/(ASCE)1090-0268(2002)6:2(73).

[5] Endeshaw MA, ElGawady M, Sack RL, McLean DI, Ghasemi H. Retrofit of Rectangular Bridge Columns Using CFRP Wrapping. MS Thesis, Department of Civil and Environmental Engineering, Washington State University; 2008.

[6] Nordin H. Strengthening structures with externally prestressed tendons: literature review. Luleå tekniska universitet; 2005.

[7] Haghani R, Al-Emrani M, Kliger R. A new method for strengtheng concrete structures using prestressed FRP laminates. ISEC 2015 - 8th Int. Struct. Eng. Constr. Conf. Implement. Innov. Ideas Struct. Eng. Proj. Manag., 2015, p. 1153–8.

[8] Ozcan O, Binici B, Ozcebe G. Improving seismic performance of deficient reinforced concrete columns using carbon fiber-reinforced polymers. Eng Struct 2008;30:1632–46. doi:10.1016/j.engstruct.2007.10.013.

[9] Abdelrahman K, El-Hacha R. Behavior of Large-Scale Concrete Columns Wrapped with CFRP and SFRP Sheets. J Compos Constr 2012;16:430–9. doi:10.1061/(ASCE)CC.1943-5614.0000278.

[10] Campione G, Cannella F, Ferrotto MF, Gianquinto M. Compressive behavior of FRP externally wrapped RC column with buckling effects of longitudinal bars. Eng Struct 2018;168:809–18.

[11] Parvin A, Brighton D. FRP composites strengthening of concrete columns under various loading conditions. Polymers (Basel) 2014;6:1040–56. doi:10.3390/polym6041040.

[12] Di Ludovico M, Prota A, Manfredi G, Cosenza E. Seismic strengthening of an under-designed RC structure with FRP. Earthq Eng Struct Dyn 2008;37:141–62. doi:10.1002/eqe.749.

[13] Eslami A, Ronagh HR. Effect of FRP wrapping in seismic performance of RC buildings with and without special detailing - A case study. Compos Part B Eng 2013;45:1265–74. doi:10.1016/j.compositesb.2012.09.031.

[14] Cao V Van, Ronagh HR. Reducing the seismic damage of reinforced concrete frames using FRP confinement. Compos Struct 2014;118:403–15. doi:10.1016/j.compstruct.2014.07.038.

[15] Niroomandi A, Maheri A, Maheri MR, Mahini SS. Seismic performance of ordinary RC frames retrofitted at joints by FRP sheets. Eng Struct 2010;32:2326–36. doi:10.1016/j.engstruct.2010.04.008.

[16] Bertero RD, Bertero V V. Performance-based seismic engineering: The need for a reliable conceptual comprehensive approach. Earthq Eng Struct Dyn 2002;31:627–52. doi:10.1002/eqe.146.

[17] Zaker Esteghamati M, Banazadeh M, Huang Q. The effect of design drift limit on the seismic performance of RC dual high-rise buildings. Struct Des Tall Spec Build 2018:e1464. doi:10.1002/tal.1464.
[18] Masoomi H, van de Lindt JW. Restoration and functionality assessment of a community subjected to tornado hazard. Struct Infrastruct Eng 2018;14:275–91. doi:10.1080/15732479.2017.1354030.
[19] Yamakawa T, Banazadeh M, Fujikawa S. Emergency retrofit of shear damaged extremely short RC columns using pre-tensioned aramid fiber belts. J Adv Concr Technol 2005;3:95–106.
[20] Sonnenschein R, Gajdosova K, Holly I. FRP Composites and their Using in the Construction of Bridges. Procedia Eng 2016;161:477–82.
[21] Parghi A, Alam MS. Seismic collapse assessment of non-seismically designed circular RC bridge piers retrofitted with FRP composites. Compos Struct 2017;160:901–16. doi:10.1016/j.compstruct.2016.10.094.
[22] Tsonos AG. Effectiveness of CFRP-jackets and RC-jackets in post-earthquake and pre-earthquake retrofitting of beam-column subassemblages. Eng Struct 2008;30:777–93. doi:10.1016/j.engstruct.2007.05.008.
[23] Yuksel E, Ozkaynak H, Buyukozturk O, Yalcin C, Dindar AA, Surmeli M, et al. Performance of alternative CFRP retrofitting schemes used in infilled RC frames. Constr Build Mater 2010;24:596–609. doi:10.1016/j.conbuildmat.2009.09.005.
[24] Aravind N, Samanta AK, Thanikal J V., Singha Roy DK. An experimental study on the effectiveness of externally bonded corrugated GFRP laminates for flexural cracks of RC beams. Constr Build Mater 2017;136:348–60. doi:10.1016/j.conbuildmat.2017.01.047.
[25] Saleem MU, Numada M, Amin MN, Meguro K. Seismic response of PP-band and FRP retrofitted house models under shake table testing. Constr Build Mater 2016;111:298–316. doi:10.1016/j.conbuildmat.2016.02.073.
[26] Caratelli A, Meda A, Rinaldi Z, Spagnuolo S, Maddaluno G. Optimization of GFRP reinforcement in precast segments for metro tunnel lining. Compos Struct 2017;181:336–46. doi:10.1016/j.compstruct.2017.08.083.
[27] Kong X, Qi X, Gu Y, Lawan IA, Qu Y. Numerical evaluation of blast resistance of RC slab strengthened with AFRP. Constr Build Mater 2018;178:244–53.
[28] Shinozaki H, Pandey GR, Mutsuyoshi H, Aravinthan T. AFRP retrofitting of RC structures in Japan. Proc. 20th Australas. Conf. Mech. Struct. Mater., Taylor & Francis (CRC Press); 2008, p. 411–7.
[29] Lau D, Qiu Q, Zhou A, Chow CL. Long term performance and fire safety aspect of FRP composites used in building structures. Constr Build Mater 2016;126:573–85. doi:10.1016/j.conbuildmat.2016.09.031.
[30] Pearson M, Donchev T, Limbachiya M. An investigation into the sustainability of FRP reinforcement bars. Proc. Fourth Int. Conf. Durab. Sustain. Fiber-Reinforced Polym. Compos. Constr. Rehabil. Quebec, QC, Canada, 2011, p. 20–2.
[31] American Society of Civil Engineers. Minimum design loads for buildings and other structures, ASCE standard,. ASCE Stand 2010:608. doi:10.1061/9780784412916.
[32] ACI Committee 318. Building Code Requirements for Structural Concrete (ACI 318-08). vol. 2007. 2008. doi:10.1016/0262-5075(85)90032-6.
[33] Mazzoni S, McKenna F, Scott MH, Fenves GL. OpenSees command language manual. Pacific Earthq Eng Res Cent 2007:451.

[34] Banazadeh M, Yamakawa T. Nonlinear cyclic analysis of shear/flexure behavior in RC columns retrofitted by pre-tensioned aramid fiber belts. J Struct Constr Eng (Transactions AIJ) 2005;70:181–8.
[35] Zuanfeng P, Bing L. Truss-Arch Model for Shear Strength of Shear-Critical Reinforced Concrete Columns. J Struct Eng 2013;139:548–60. doi:10.1061/(ASCE)ST.1943-541X.0000677.
[36] Mander JB, Priestley MJN, Park R. Theoretical stress-strain model for confined concrete. J Struct Eng 1988;114:1804–26. doi:10.1061/(ASCE)0733-9445(1988)114:8(1804).
[37] Richart F, Brandtzaeg A, Brown RL. A Study of the Failure of Concrete under Combined Compressive Stresses. Univ Illinois Bull 1928;26, Bullet:1–104.
[38] Haselton CB, Liel AB, Lange ST. Beam-Column Element Model Calibrated for Predicting Flexural Response Leading to Global Collapse of RC Frame Buildings. Peer 2007 2008;03.
[39] Lowes LN, Mitra N, Altoontash A. A Beam-Column Joint Model for Simulating the Earthquake Response of Reinforced Concrete Frames A Beam-Column Joint Model for Simulating the Earthquake Response of Reinforced Concrete Frames, PEER Report 2003/10. 2004.
[40] Zareian F, Medina RA. A practical method for proper modeling of structural damping in inelastic plane structural systems. Comput Struct 2010;88:45–53. doi:10.1016/j.compstruc.2009.08.001.
[41] Vamvatsikos D, Allin Cornell C. Incremental dynamic analysis. Earthq Eng Struct Dyn 2002;31:491–514. doi:10.1002/eqe.141.
[42] Federal Emergency Management Agency. Quantification of building seismic performance factors FEMA P695. 2009.
[43] Vamvatsikos D, Cornell CA. Applied incremental dynamic analysis. Earthq Spectra 2004;20:523–53. doi:10.1193/1.1737737.
[44] American Society of Civil Engineers (ASCE). FEMA 356 Prestandard and Commentary for the Seismic Rehabilitation of Building. Rehabilitation 2000.
[45] Baker JW. Efficient analytical fragility function fitting using dynamic structural analysis. Earthq Spectra 2015;31:579–99. doi:10.1193/021113EQS025M.
[46] Goulet CA, Haselton CB, Mitrani-Reiser J, Beck JL, Deierlein GG, Porter KA, et al. Evaluation of the seismic performance of a code-conforming reinforced-concrete frame building - From seismic hazard to collapse safety and economic losses. Earthq Eng Struct Dyn 2007;36:1973–97. doi:10.1002/eqe.694.
[47] Haselton CB, Deierlein GG. Assessing seismic collapse safety of modern reinforced concrete moment frame buildings. Berkeley: PEER; 2007.
[48] Ronagh HR, Eslami A. Flexural retrofitting of RC buildings using GFRP/CFRP - A comparative study. Compos Part B Eng 2013. doi:10.1016/j.compositesb.2012.09.072.
[49] Toutanji H, Deng Y. Strength and durability performance of concrete axially loaded members confined with AFRP composite sheets. Compos Part BEngineering 2002;33:255–61. doi:10.1016/S1359-8368(02)00016-1.
[50] Kumutha R, Vaidyanathan R, Palanichamy MS. Behaviour of reinforced concrete rectangular columns strengthened using GFRP. Cem Concr Compos 2007;29:609–15. doi:10.1016/j.cemconcomp.2007.03.009.
[51] Promis G, Ferrier E. Performance indices to assess the efficiency of external FRP retrofitting of reinforced concrete short columns for seismic strengthening. Constr Build

Mater 2012;26:32–40. doi:10.1016/j.conbuildmat.2011.04.067.
[52] Tabandeh A, Gardoni P. Probabilistic capacity models and fragility estimates for RC columns retrofitted with FRP composites. Eng Struct 2014;74:13–22. doi:10.1016/j.engstruct.2014.05.005.
[53] Seyhan EC, Goksu C, Uzunhasanoglu A, Ilki A. Seismic behavior of substandard RC columns retrofitted with embedded Aramid Fiber Reinforced Polymer (AFRP) reinforcement. Polymers (Basel) 2015;7:2535–57. doi:10.3390/polym7121527.
[54] Dundar C, Erturkmen D, Tokgoz S. Studies on carbon fiber polymer confined slender plain and steel fiber reinforced concrete columns. Eng Struct 2015;102:31–9. doi:10.1016/j.engstruct.2015.08.011.
[55] Rodsin K. Brittle shear failure prevention of a non-ductile RC column using glass fiber reinforced polymer (GFRP). Procedia Eng., vol. 125, 2015, p. 911–7. doi:10.1016/j.proeng.2015.11.091.

Table 1. Literature summary of FRP effect on RC column

Reference	Year	summary
Toutanji and Deng [49]	2002	AFRP sheet increased concrete compressive strength up to 220%
Kumutha et al. [50]	2007	GFRP increased load carrying capacity of columns but this increase depends on the number of GFRP layers and columns cross sections
Promis et al.[51]	2009	FRP reinforcement shifted brittle shear failure mode to ductile flexural failure for fully wrapped columns. All Columns retrofitted with FRP had higher ultimate load and displacement capacity than reference column
Tabandeh and Gardoni [52]	2014	They showed that although FRP improved fragility curve of columns, it was more effective for columns that were not seismically designed
Seyhan et al. [53]	2015	The flexural strength of columns retrofitted with AFRP, were about 38% to 91% higher than reference column
Dundar et al.[54]	2015	using CFRP sheets in transverse and longitudinal directions increased ductility and ultimate strength of both plain and reinforced concrete
Rodsin [55]	2015	Non-ductile column failed in shear at a drift value of 3.5%, whereas the column failed in flexure at a drift value of 12%

Table 2. Equivalent lateral force analysis of buildings

Model	Height (m)	W (ton)	T_1 (s)	C_s	Base shear (ton)
4-story	12.8	1267.8	0.65	0.18	223.10
6-story	19.2	2021.1	0.94	0.12	246.57
8-story	25.6	2866.9	1.20	0.09	269.49

Table 3. The beams and columns sections of the designed buildings

Model	Story No.	Beams	Long. Reinf.		Trans. ties	Inner column	Long Reinf.	Trans ties	Outer column	Long. Reinf.	Trans ties
4-story	**1**	50X60	Top	4φ25	2φ10/17	60X60	16φ25	2φ8/35	60X60	16φ25	2φ8/35
			Bottom	4φ25							
	2	50X60	Top	4φ28	2φ10/14	50X50	12φ25	2φ8/30	50X50	12φ25	2φ8/30
			Bottom	4φ28							
	3	40X50	Top	4φ25	2φ8/13	50X50	12φ25	2φ8/30	50X50	12φ25	2φ8/30
			Bottom	3φ25							
	4	40X50	Top	3φ22	2φ8/18	45X45	8φ26	2φ8/25	45X45	8φ26	2φ8/25
			Bottom	3φ22							
6-story	**1**	60X70	Top	4φ26	2φ8/16	60X60	16φ28	2φ10/3	60X60	16φ28	2φ10/30
			Bottom	3φ26							
	2	60X70	Top	5φ26	2φ8/14	50X50	12φ25	2φ10/3	60X60	16φ28	2φ10/30
			Bottom	4φ26							
	3	60X70	Top	5φ26	2φ8/12	50X50	12φ25	2φ10/3	60X60	16φ28	2φ10/30
			Bottom	4φ26							
	4	50X60	Top	5φ25	2φ8/17	50X50	12φ25	2φ10/3	60X60	16φ28	2φ10/30
			Bottom	4φ25							
	5	50X60	Top	5φ22	2φ8/25	50X50	12φ25	2φ10/3	50X50	12φ25	2φ10/30
			Bottom	4φ22							
	6	50X60	Top	4φ22	2φ8/30	40X40	8φ18	2φ8/35	45X45	8φ25	2φ8/35
			Bottom	3φ22							
8-story	**1**	60X70	Top	5φ26	2φ10/10	70X70	16φ28	2φ10/3	70X70	16φ28	2φ10/35
			Bottom	4φ26							
	2	60X70	Top	5φ28	2φ10/7.5	60X60	16φ26	2φ10/2	70X70	16φ28	2φ10/35
			Bottom	4φ28							
	3	60X70	Top	5φ28	2φ10/7.5	60X60	16φ26	2φ10/2	60X60	16φ26	2φ10/25
			Bottom	3φ28							
	4	60X70	Top	5φ28	2φ10/8	60X60	16φ26	2φ10/2	60X60	16φ26	2φ10/25
			Bottom	3φ28							
	5	50X60	Top	5φ25	2φ10/7	60X60	16φ26	2φ10/2	60X60	16φ26	2φ10/25
			Bottom	3φ25							
	6	50X60	Top	5φ25	2φ10/7	45X45	8φ22	2φ8/25	60X60	16φ26	2φ10/25
			Bottom	3φ25							
	7	50X60	Top	5φ22	2φ8/10	50X50	12φ20	2φ8/30	60X60	16φ26	2φ10/25
			Bottom	3φ22							
	8	50X60	Top	5φ18	2φ8/18	45X45	8φ22	2φ8/25	50X50	12φ20	2φ8/30
			Bottom	3φ18							

Table 4. The results of IDA and pushover analysis

Building		Ω	μ_T	Sa_{MCE} (g)	$S_{a\,Col}$ (g)	IDR_{col}	$P[C|Sa_{MCE}]$	λ_{Col} ($x10^{-4}$)	$P_{C/50}$(%)
4-story	Original	3.59	0.94	1.32	1.05	0.05	0.70	14.98	7.22
	Retrofitted	4.65	2.23	1.32	2.30	0.10	0.06	2.83	1.41
6-story	Original	3.11	0.76	0.92	0.81	0.07	0.60	12.08	5.86
	Retrofitted	4.99	1.30	0.92	1.35	0.09	0.19	4.82	2.38
8-story	Original	3.41	0.77	0.71	0.73	0.07	0.46	9.04	4.42
	Retrofitted	4.94	2.27	0.71	1.34	0.10	0.03	3.03	1.50

Table 5. Comparison of median IDA results corresponding to different limit states

model		IO	LS	CP	Collapse
4-story	Original	0.30	0.55	0.79	1.12
	Retrofitted	0.30	0.52	0.87	1.86
6-story	Original	0.20	0.30	0.53	0.75
	Retrofitted	0.20	0.34	0.65	1.11
8-story	Original	0.14	0.29	0.50	0.67
	Retrofitted	0.14	0.29	0.68	1.03

(*) the values are in units of g.

Table 6. FEMA P695 assessment results

model		CMR	SSF	ACMR	βtotal	$ACMR_{allowable}$	Pass/Fail
4-story	Original	.83	.99	.82	.40	1.48	Fail
	Retrofitted	1.45	1.19	1.73	.47	1.68	Pass
6-story	Original	.82	.96	.79	.39	1.47	Fail
	Retrofitted	1.24	1.06	1.31	.42	1.55	Fail
8-story	Original	.94	.96	.90	.39	1.47	Fail
	Retrofitted	1.52	1.26	1.92	.48	1.69	Pass

Table 7. Median values of structural component's ductility

model	Story No.	DBE				MCE				collapse			
		columns		beams		columns		beams		columns		beams	
		org	ret	org	ret	org	ret	org	ret	org	ret	org	ret
4-story	1	1.39	1.07	8.34	7.52	1.56	2.21	7.08	19.26	1.49	1.40	9.44	11.12
	2	3.32	5.75	1.81	1.21	3.42	12.16	1.34	2.27	3.37	7.52	1.63	1.53
	3	1.49	2.48	3.27	5.28	1.58	4.78	3.12	12.94	1.45	2.96	3.03	7.78
	4	2.16	3.19	1.91	1.59	2.25	8.45	1.39	3.96	2.39	4.58	1.93	2.20
6-story	1	0.63	1.67	1.4	27.11	0.66	2.04	1.38	34.32	0.64	2.52	1.55	39.50
	2	1.78	3.24	0.80	11.91	1.87	4.03	0.81	17.66	2.04	4.73	0.91	20.73
	3	0.85	2.71	0.87	3.91	0.87	3.58	0.89	6.59	0.9	3.99	0.91	7.56
	4	0.72	1.07	0.83	2.39	0.75	1.31	0.85	4.56	0.75	1.37	0.89	4.89
	5	1.01	1.67	0.76	0.89	1.08	1.94	0.78	1.02	1.10	2.07	0.82	1.01
	6	2.37	4.92	0.35	0.39	2.68	6.11	0.36	0.41	2.48	6.27	0.42	0.41
8-story	1	0.67	1.45	3.9	21.39	0.71	2.41	0.85	34.51	0.71	3.26	6.75	45.63
	2	1.06	1.87	0.86	12.92	1.13	2.91	5.45	23.03	1.24	3.68	3.91	30.79
	3	1.00	2.43	0.72	5.27	1.18	4.07	2.77	10.81	1.26	5.03	2.97	16.57
	4	0.81	1.61	0.72	2.20	0.83	2.33	1.76	4.56	0.93	2.99	1.66	7.21
	5	0.72	0.99	1.51	6.48	0.75	1.36	0.75	8.30	0.78	1.62	2.02	11.93
	6	1.96	2.51	2.14	9.34	2.44	2.87	0.73	9.61	2.38	3.67	2.82	13.04
	7	0.83	1.33	4.38	10.10	0.87	1.7	0.88	13.84	0.92	2.04	4.60	19.49
	8	1.70	2.57	0.83	1.00	1.86	3.49	4.10	1.00	1.87	4.11	0.82	1.27

Table 8. Sum of structural components' dissipated energy

model	Story No.	DBE				MCE				collapse			
		columns		beams		columns		beams		columns		beams	
		org	ret	org	ret	org	ret	org	ret	org	ret	org	ret
4-story	1	5.83	1.83	21.12	20.83	8.29	2.74	22.74	18.67	5.44	8.34	19.19	10.15
	2	22.15	33.24	14.68	10.62	21.09	37.33	12.57	7.36	22.16	43.46	16.68	4.33
	3	5.85	11.05	17.86	12.84	6.48	11.97	14.81	11.03	5.49	13.33	16.03	7.50
	4	9.71	7.24	2.79	2.33	9.53	9.32	4.49	1.58	11.23	11.92	3.79	0.97
6-story	1	2.61	5.42	51.11	37.2	2.37	7.77	47.83	29.65	2.66	9.17	46.83	27.07
	2	25.04	9.72	2.03	23.68	25.31	10.76	3.05	23.24	29.28	11.49	2.44	23.90
	3	1.10	4.18	0.01	5.59	0.97	5.05	0.01	7.06	1.20	5.64	0.01	7.45
	4	0.60	0.28	0.11	1.38	0.53	0.39	0.13	3.10	0.60	0.39	0.14	2.90
	5	1.82	1.88	0.07	0.49	1.90	2.34	0.14	1.20	1.78	2.3	0.11	1.09
	6	15.51	10.19	<0.01	<0.01	17.76	9.45	<0.01	<0.01	14.93	8.61	<0.01	<0.01
8-story	1	1.53	3.60	34.92	24.42	1.19	6.68	27.11	18.9	1.19	9.4	28.31	15.32
	2	1.98	1.60	21.26	24.58	2.19	2.63	22.87	24.99	2.12	3.06	22.8	23.27
	3	1.66	4.37	12.77	8.28	2.18	6.30	16.58	11.30	2.08	6.51	16.24	12.46
	4	0.47	1.75	1.44	3.07	0.52	2.40	4.17	3.36	0.49	2.91	4.00	4.63
	5	0.26	0.59	2.09	8.50	0.19	0.54	3.41	6.90	0.20	0.70	2.90	6.90
	6	5.32	2.31	5.17	8.46	5.52	1.92	4.76	6.33	5.49	2.10	4.80	5.69
	7	0.28	0.43	7.22	5.88	0.21	0.41	6.31	5.05	0.22	0.43	6.30	4.61
	8	3.63	2.15	<0.01	<0.01	2.78	2.30	<0.01	<0.01	2.87	2.03	<0.01	<0.01

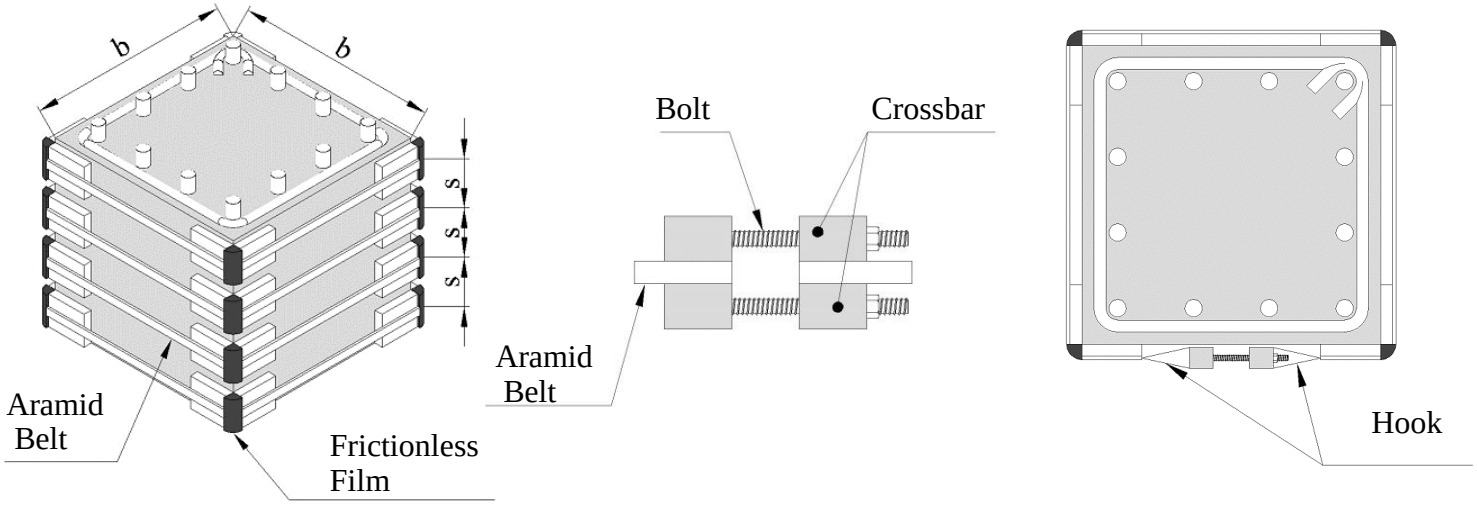

Figure 1. Details of AFRP retrofitting

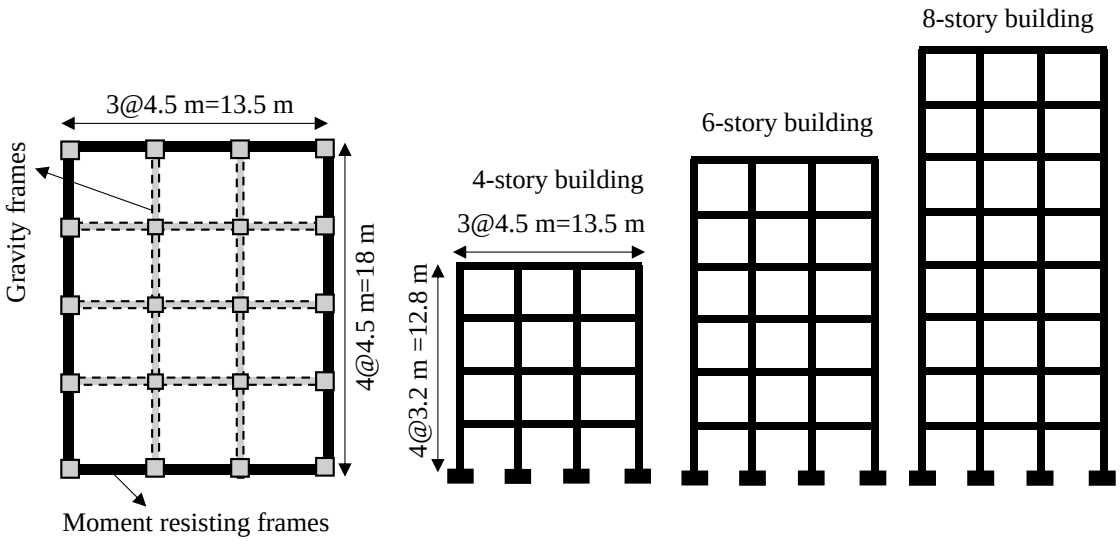

Figure 2. Typical plan and elevation of building

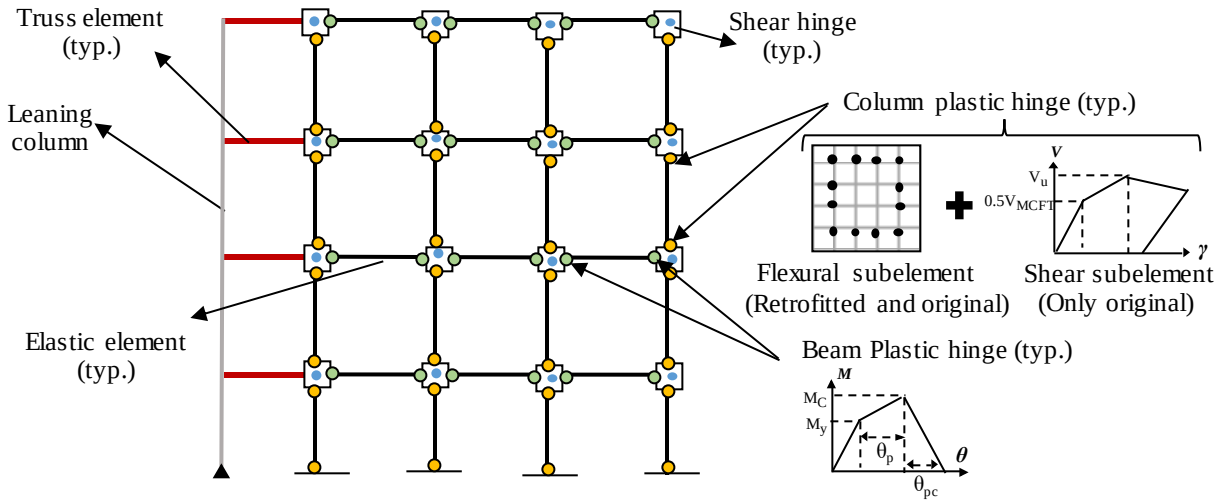

Figure 3. Typical finite element model configuration

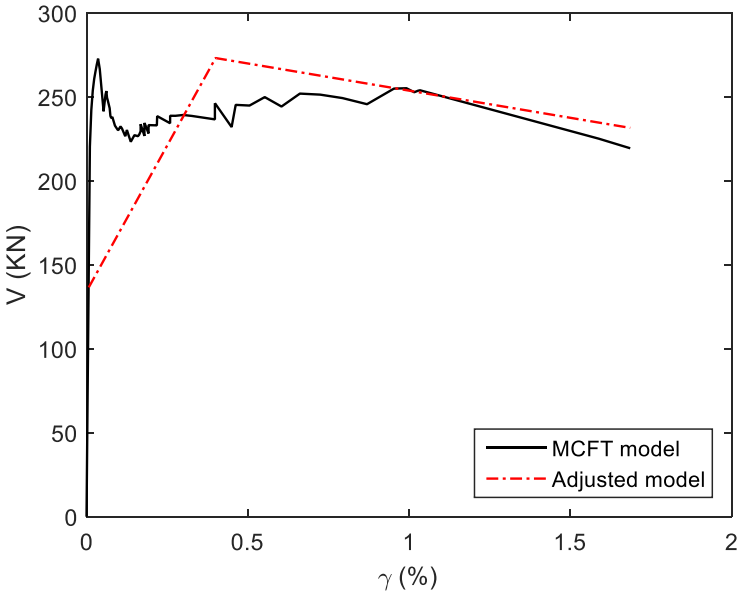

Figure 4. The modification of shear-distortion behavior obtained from MCFT model of a 50cmX50cm column of 4-sotry model

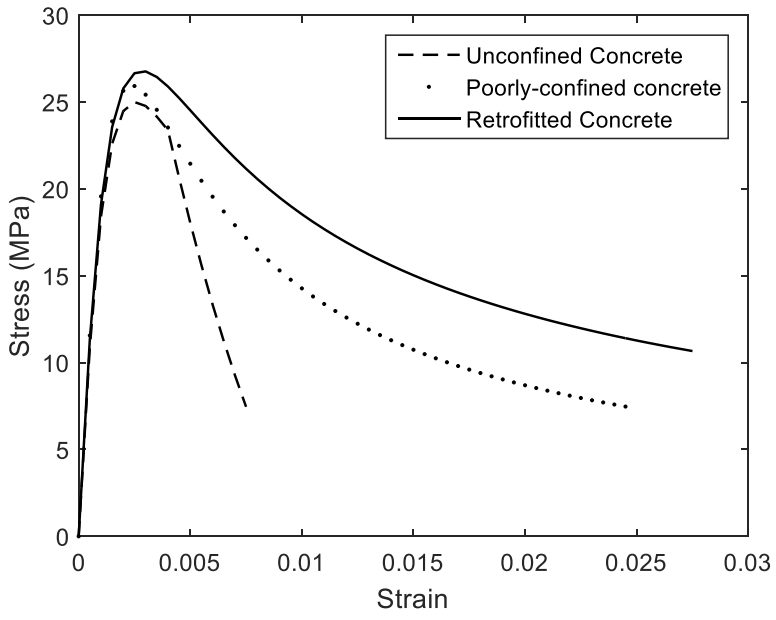

Figure 5. The effect of different confinement sources on the stress -strain behavior of a 50cmX50cm column

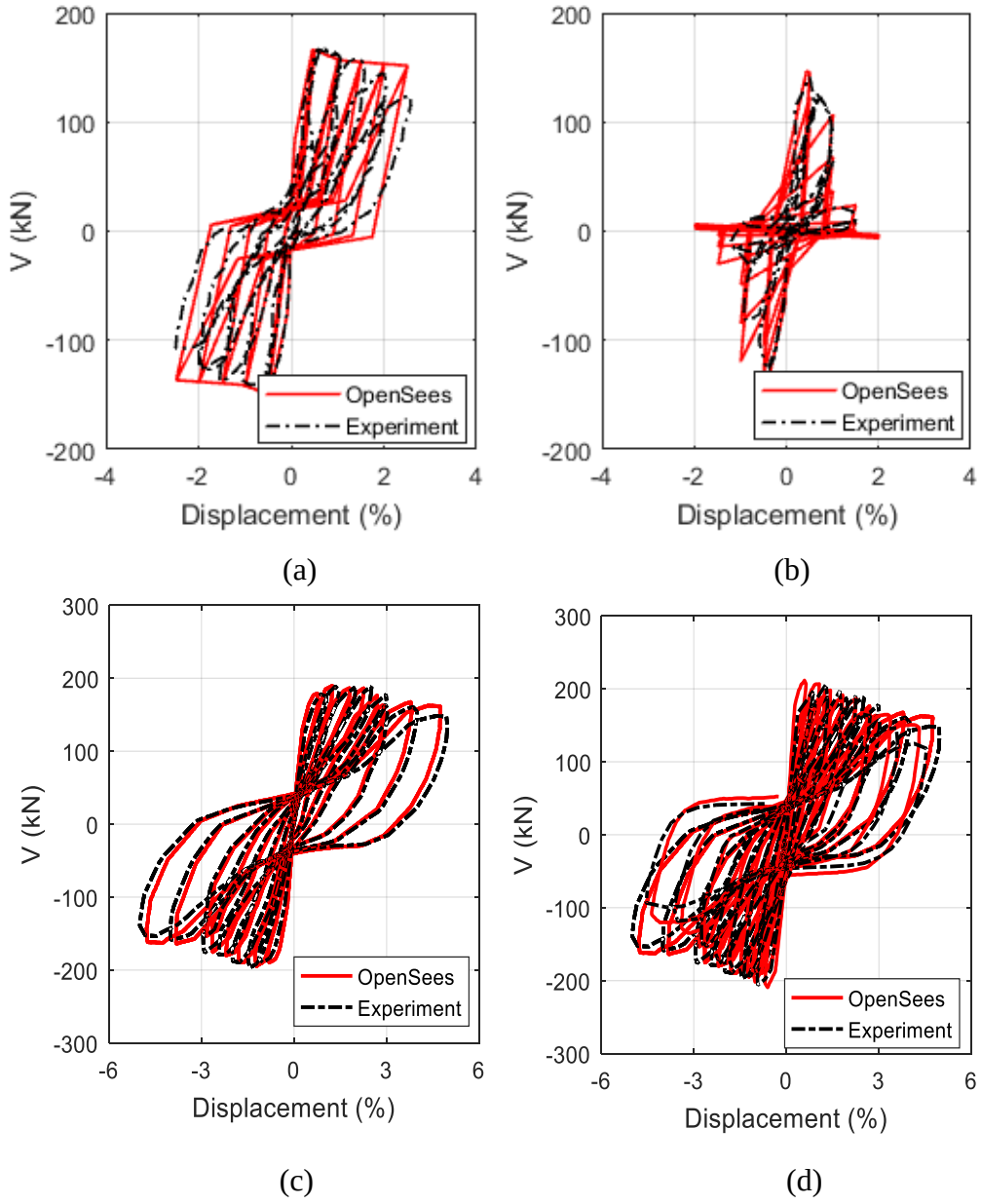

Figure 6. Comparison of OpenSees and experimental results for (a) A200/3 (b) A0 (c) A65/2 and (d) A65/3

/

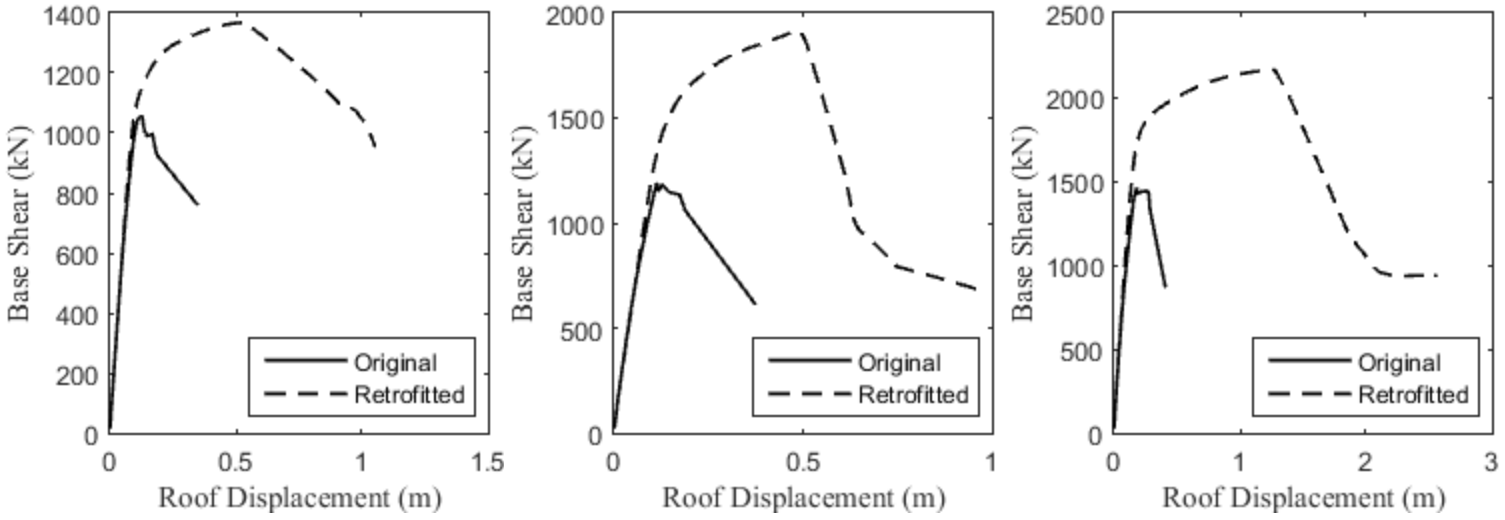

Figure 7. Pushover curves of (a) 4- (b) 6- and (c) 8-story buildings

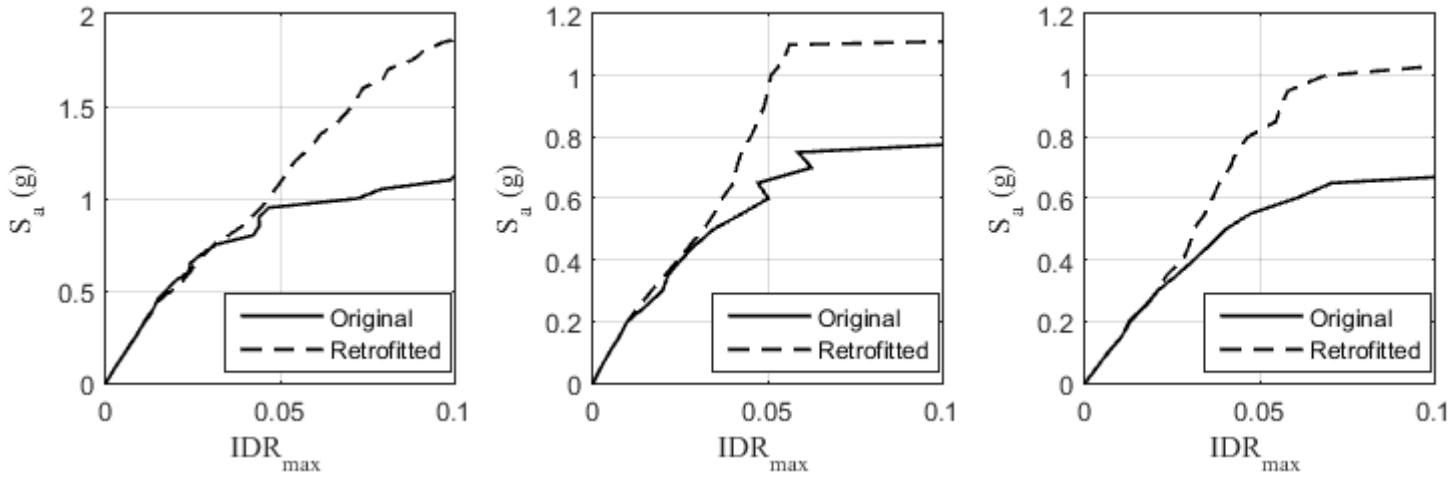

Figure 8. Median IDA curves of (a) 4- (b) 6- and (c) 8-story buildings

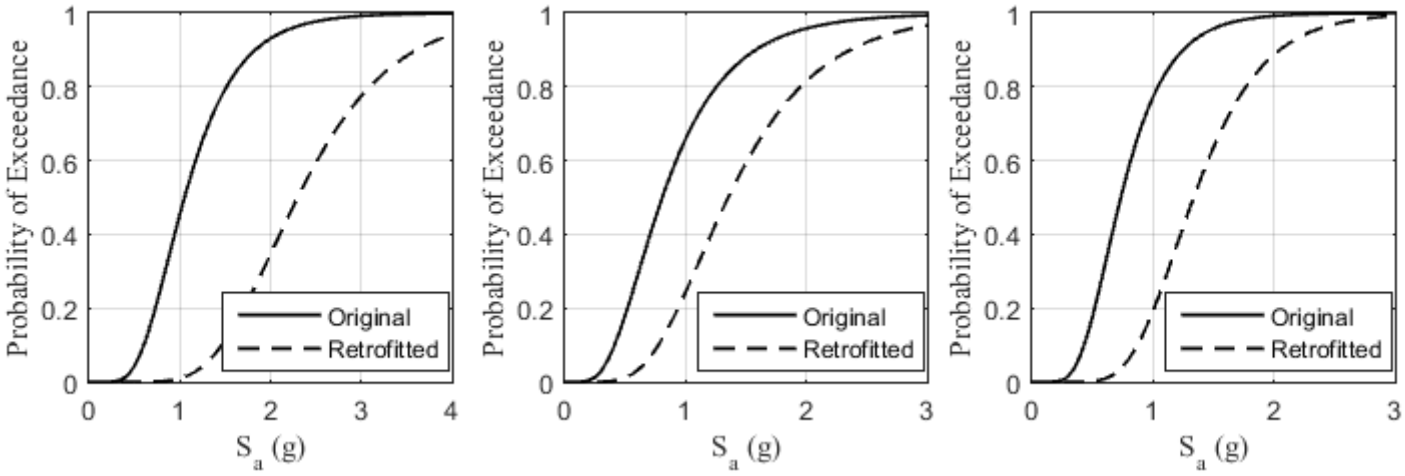

Figure 9. Collapse fragility curves of (a) 4- (b) 6- and (c) 8-story buildings

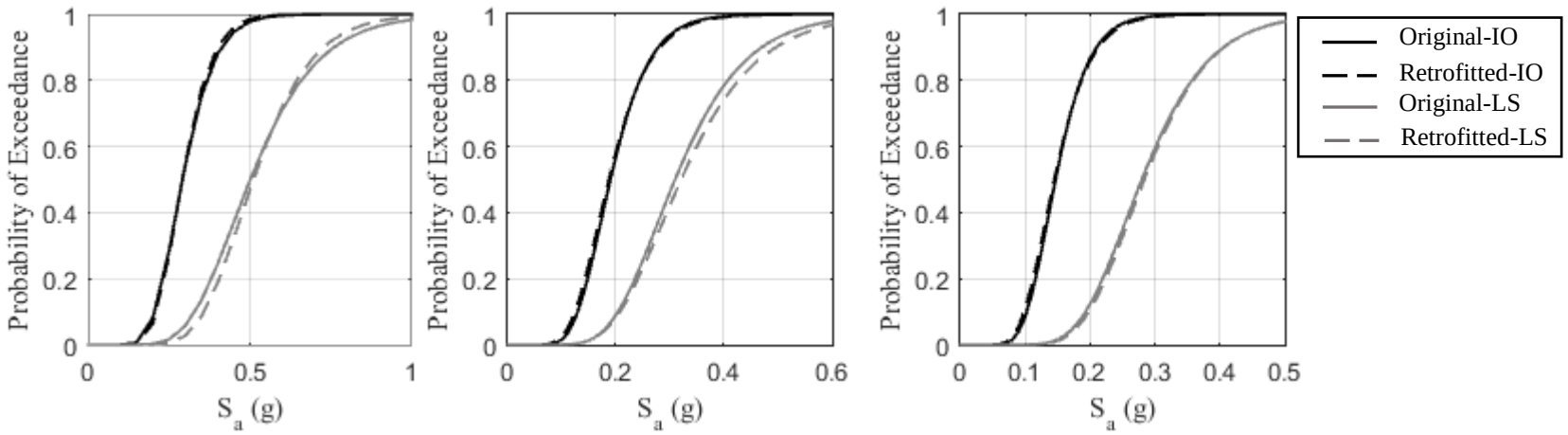

(a) (b) (c)

Figure 10. IO and LS fragility curves of (a) 4- (b) 6- and (c) 8-story buildings

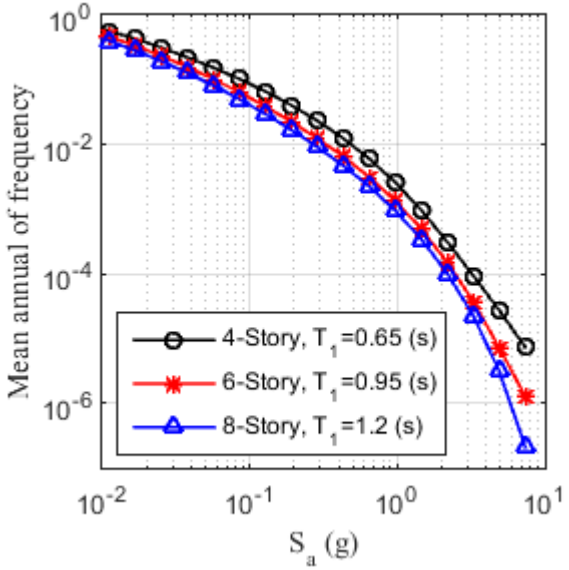

Figure 11. Spectral acceleration hazard curves of all buildings

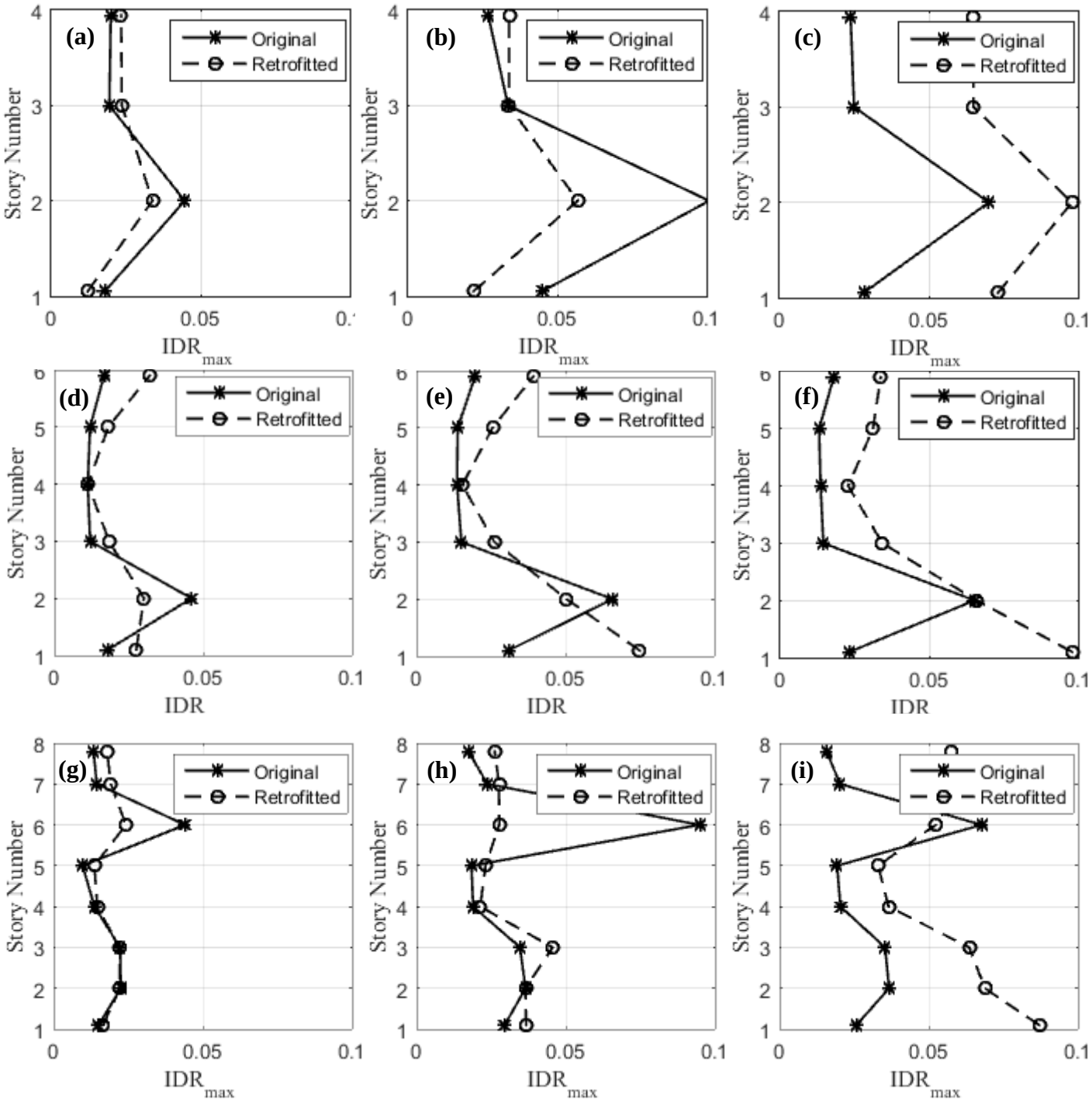

Figure 12. Median drift distribution of archetype buildings. (a) to (c), (d) to (f) and (g) to (i) show the median drift distribution of the 4-, 6- and 8-story models under DBE, MCE and collapse, respectively.